JOURNAL OF MATERIALS SCIENCE 30 (1995) 970–979

Microstructure and crack sensitivity of laser-fusion zones of Ti–46 mol % Al–2 mol % Mo alloy

A. HIROSE, Y. ARITA, K. F. KOBAYASHI
Department of Welding and Production Engineering, Faculty of Engineering, Osaka University, 2-1, Yamadaoka, Suita, Osaka 565, Japan

Laser surface melting and laser welding were performed on Ti–46 mol % Al–2 mol % Mo using a 2.5 kW CO_2 laser. Microstructures of the fusion zones were changed in the following way as the cooling rate increased:

massive α_2 + massive γ + lamellar($\alpha_2 + \gamma$) → massive α_2 + massive γ → α_2.

In laser surface melting, a single-phase structure of α_2 was seen when the calculated average cooling rates between 1773 and 1273 K were above approximately 4000 K s^{-1}. In laser welding, the microstructure of the fusion zones was mainly composed of massive α_2 + massive γ + lamellar. The hardness of the fusion zones increased with increasing cooling rate and the single-phase structure of α_2 showed hardness above 500 Hv. While all of the laser surface-melted zones included cracking, in laser welding, crack-free welds could be obtained at traverse speeds below 50.0 mm s^{-1} and pre-heating temperatures above 573 K. As a result, cracking was prevented by selecting optimum welding parameters which result in calculated cooling rates between 1073 and 873 K below approximately 30 K s^{-1} and the hardness of the fusion zones below approximately 400 Hv. In tensile tests, the laser-welded specimens without weld cracking fractured in the base metal. Thus, laser welding can be applied to the joining of Ti–46 mol % Al–2 mol % Mo.

1. Introduction

There have been increasing demands for lightweight high-temperature materials. The intermetallic compound γ-TiAl is an attractive material for the elevated temperature applications because of its low density, high modulus and relatively good oxidation resistance. However, its low ductility at room temperature has prevented practical applications. It has been reported that the room-temperature toughness was improved by the addition of ternary alloying elements [1–3]. Thus, the disadvantages in mechanical properties of TiAl alloys are being overcome by metallurgical efforts. Another problem in structural applications of TiAl alloys is secondary processing, such as cutting, joining, surface modification, etc. For the secondary processing of the TiAl alloys, it is desirable to apply fusion processes, i.e. fusion welding, surface melting, alloying, cladding and so on, because these processes are convenient and cost-effective processes from the engineering stand point. However, few works have addressed the fusion processes of TiAl alloys [4]. To investigate the applicability of fusion processing to TiAl alloys, a basic understanding of the microstructures of rapidly solidified fusion zones, which is related to their crack sensitivity, is required.

In the present work, a molybdenum-doped TiAl alloy (Ti–46 mol % Al–2 mol % Mo) was used. The addition of molybdenum has been reported to improve room-temperature ductility and high-temperature oxidation resistance of the TiAl alloys [3]. Because a laser beam is the most controllable and flexible heat source for fusion material processing, we examined laser processing of the TiAl alloy. Laser surface melting and laser welding were performed on the TiAl alloy using a 2.5 kW CO_2 laser with varying traverse speed. Thus, fusion zones subjected to various cooling rates were obtained and their microstructures, hardness and crack sensitivities were investigated. The tensile strengths of the laser weld joints were measured.

2. Experimental procedure

2.1. Material

Ti–46 mol % Al–2 mol % Mo was prepared by argon arc melting with a non-consumable electrode. The ingot was approximately 60 mm diameter and 110 mm long. Its chemical composition is listed in Table I.

2.2. Laser surface melting

Disc specimens, 60 mm diameter and 10 mm thick, were cut from the ingot. The surface of the disc

0022–2461

TABLE I Chemical composition of TiAl alloy used

	Chemical composition (mol %)				
	Ti	Al	Mo	C	O
Ti–46 Al–2 Mo	Bal.	45.5	1.96	0.0004	0.0013

specimen was polished and cleaned with acetone before laser surface melting. The laser beam was irradiated on the surface using a laser power of 2.5 kW and traverse speeds were varied from 13.3–33.3 mm s^{-1}. The focal position was kept constant at 5 mm above the surface. The surface melting was carried out in a shielding box whose atmosphere was displaced by argon gas to prevent oxidation of the fusion zones.

2.3. Laser welding

Specimens 35 mm wide, 50 mm long and 2 mm thick, were used for laser welding. Fully penetrated bead-on-plate welding over a 35 mm length was performed using a laser power of 2.5 kW and traverse speeds varying from 25.0–83.3 m s^{-1} in the argon shielding box. The laser beam was focused just on the specimen surface. The initial temperatures of the specimens were varied from room temperature to 673 K. Pre-heating of the specimen was carried out using a hot plate.

2.4. Metallographic observations

Surface cracking in laser surface melting and laser welding was examined by means of a penetrant test. Observations of the optical microstructures of the fusion zones were performed on polished and etched cross-sections by Kroll's reagent. Vickers hardness measurements were made on the cross-sections using a load of 4.9 N. Specimens for transmission electron microscopy (TEM) were prepared from the fusion zones and were mechanically ground to a thickness of approximately 50 μm and thinned to electron transparency by an ion-milling apparatus. TEM observations and selected-area diffractions were performed using a 200 kV transmission electron microscope linked with quantitative energy-dispersive X-ray (EDX) spectroscopy. X-ray diffractometry measurements were carried out on longitudinal sections parallel to the fusion zone surfaces at a depth of approximately 500 μm.

2.5. Tensile test

Tensile specimens 50 mm long, 10 mm wide and 2 mm thick were extracted from welded plates made with a traverse speed of 33.3 m s^{-1} and a preheat temperature of 573 K. Tensile tests were performed on an Instron-type testing machine at room temperature using a cross-head speed of 8.33×10^{-3} mm s^{-1}.

3. Results

3.1. Microstructure

Fig. 1 shows the optical microstructure of the base metal. The lamellar structure containing γ(TiAl) + $\alpha_2(Ti_3Al)$, which were identified by X-ray diffractometry, was observed (Fig. 2).

Fig. 3 shows cross-sectional optical micrographs of the laser surface-melted regions. The fusion zones, produced at the traverse speeds of 33.3 and 16.7 mm s^{-1}, were hardly etched by the Kroll's reagent used, and microstructures could be barely observed with an optical microscope (Fig. 3a and b). Fine

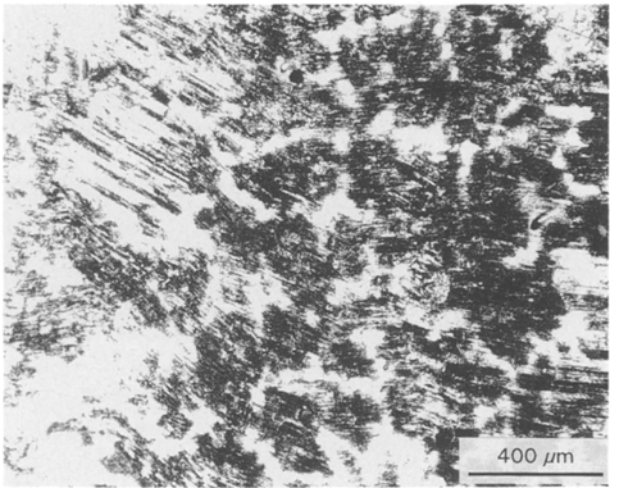

Figure 1 Optical microstructure of Ti–46 mol % Al–2 mol % Mo-base alloy.

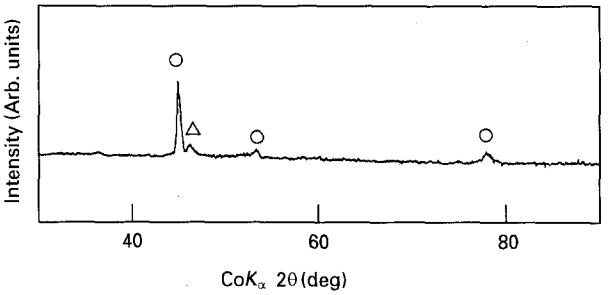

Figure 2 X-ray diffraction pattern of Ti–46 mol % Al–2 mol % Mo-base alloy. (○) γ, (△) α_2.

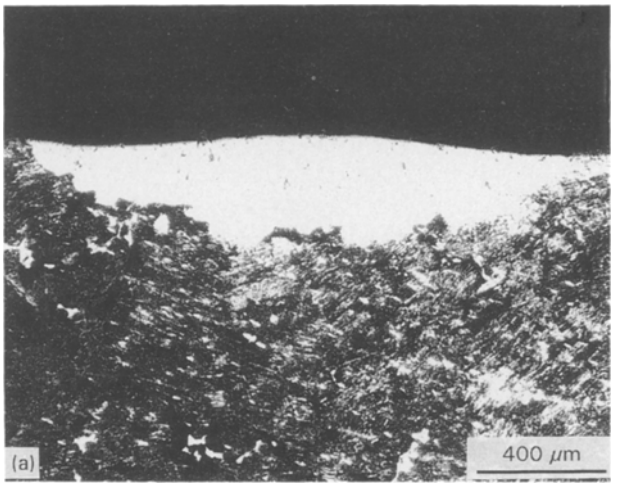

Figure 3 Cross-sectional optical micrographs of the laser surface-melted regions: traverse speeds (a) 33.3 mm s^{-1}, (b) 16.7 mm s^{-1}, (c) 13.3 mm s^{-1}.

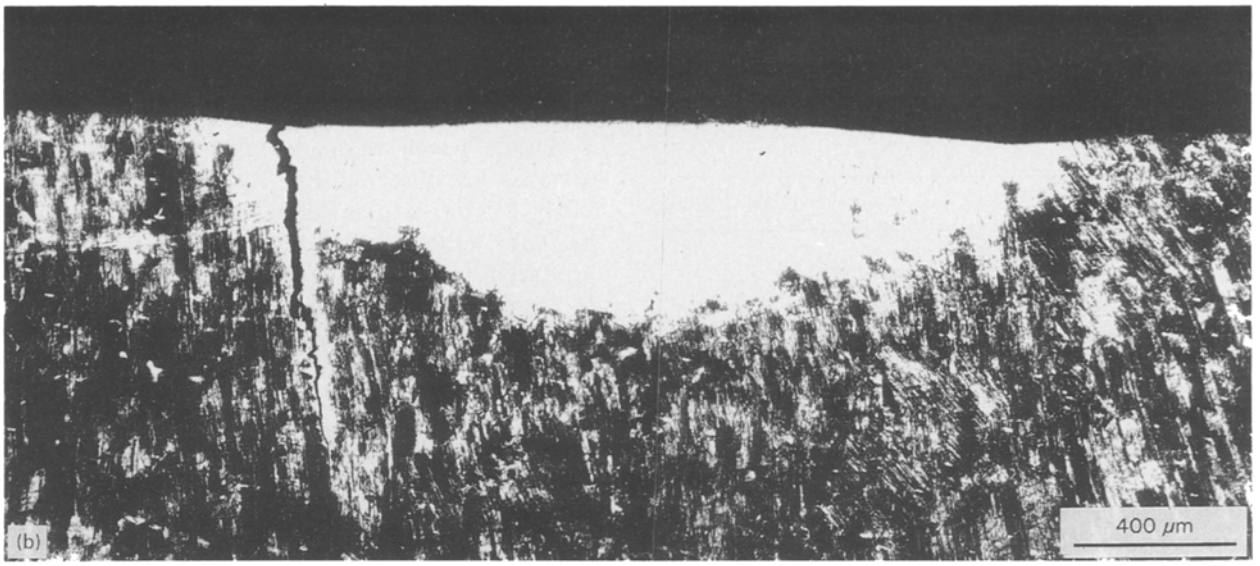

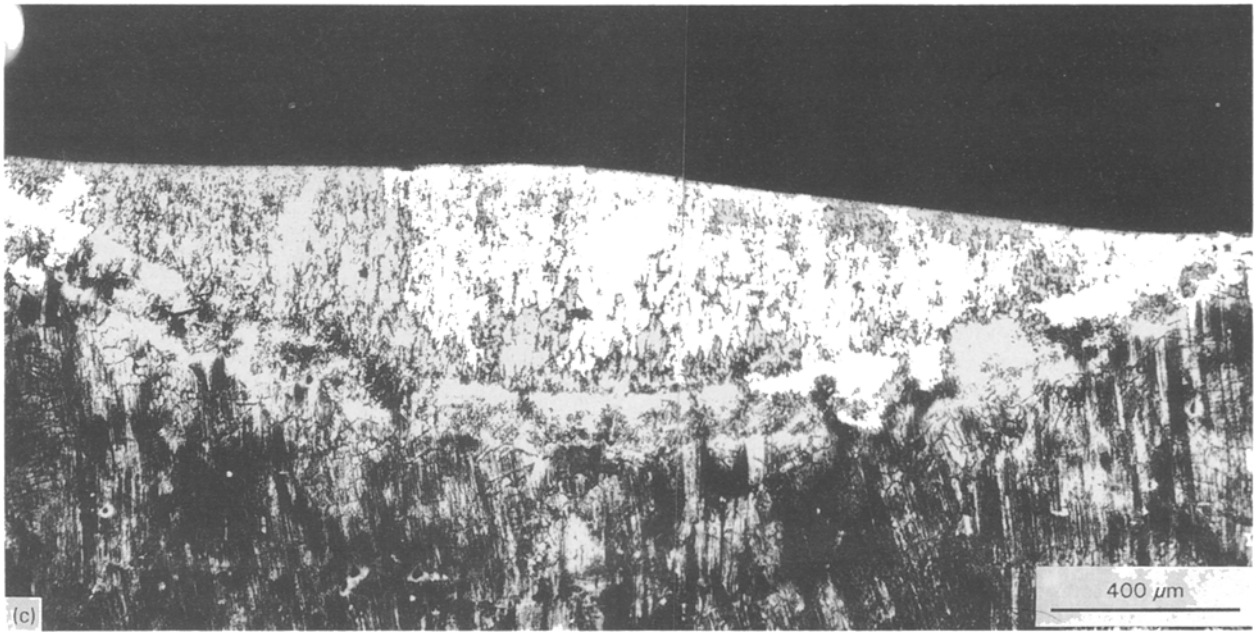

Figure 3 (Continued)

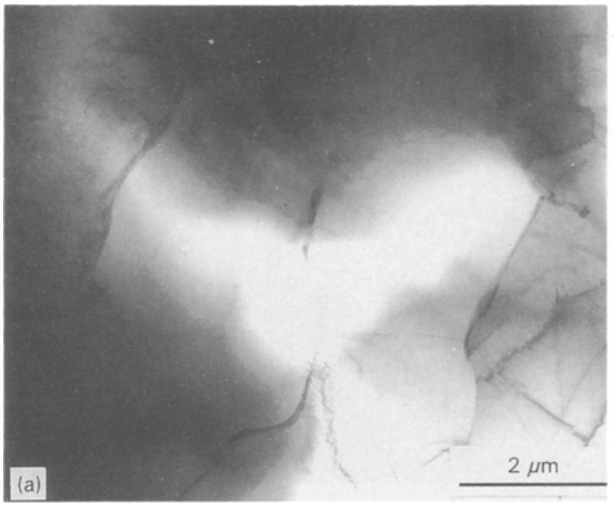

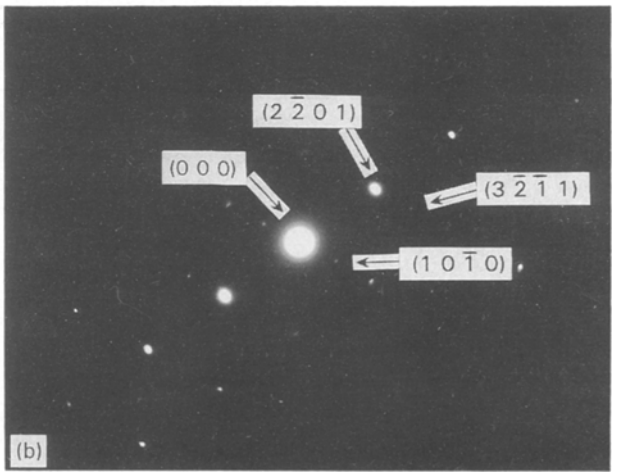

Figure 4 Transmission electron micrographs of the laser surface-melted zone (traverse speed 33.3 mm s^{-1}): (a) bright-field image of α_2 grains; (b) selected-area diffraction pattern of (a), (beam $\parallel [1\,\bar{2}\,1\,\bar{6}]_{\alpha_2}$).

microstructure, which was related to the solidification structure, was seen in the fusion zone at a slower traverse speed of 13.3 mm s^{-1}, as shown in Fig. 3c.

The microstructures of the fusion zones were observed in more detail using TEM. Fig. 4 shows a bright-field image and a selected-area diffraction of the fusion zone at a traverse speed of 33.3 mm s^{-1}. The structure consisted of α_2 fine grains, of a few micrometres in size. The chemical composition of the α_2 phase measured by EDX was 45.9 mol % Al and 2.0 mol % Mo. The composition, which is close to that of the base metal, has much higher aluminium content than the stoichiometric composition of α_2 phase. Fig. 5a shows the X-ray diffraction pattern obtained from this fusion zone. Only diffraction peaks for α_2 phase were detected. Therefore, the microstructure of the fusion zone at a traverse speed of 33.3 mm s^{-1} was found to be a single-phase structure of α_2 which was a non-equilibrium phase at the composition of the fusion zone. Fig. 5b shows the X-ray diffraction pattern obtained from the fusion zone at a traverse speed of 16.7 mm s^{-1}. Because only α_2 peaks were detected, the fusion zone structure at this traverse speed was also the single-phase structure of α_2. In the fusion zone at a traverse speed of 13.3 mm s^{-1}, γ phase was identified in addition to α_2 phase, as shown in Fig. 6. The X-ray diffraction pattern also revealed α_2 and γ peaks in this fusion zone (Fig. 5c). However, as shown in Fig. 6, they are not of the lamellar form which is observed in the base metal, but rather a massive one.

In laser welding, fully penetrated welds of which the top and bottom contours were uniform, were obtained in all of the welding conditions used in this work. Cross-sectional optical micrographs of typical laser-welded zones, which were made under three different welding conditions, are shown in Fig. 7. The bead width increased and the microstructure coarsened with decrease in the traverse speed and increase in pre-heating temperature. Detailed microstructures of the fusion zones were observed using TEM. Fig. 8 shows bright-field images and selected-area diffractions of the fusion metal at a traverse speed of 50.0 mm s^{-1} with no pre-heating. Massive α_2 (Fig. 8a and b), massive γ (Fig. 8c and d) and lamellar structure (Fig. 8e) were identified. However, only γ peaks were detected in the X-ray diffractometry of the fusion zone (Fig. 9). Thus the microstructure of the weld metal was predominantly γ phase and included massive α_2 and lamellar structure as the minor phases. The microstructure of the other weld metals also consisted of γ as the dominant phase, and α_2 and lamellar struc-

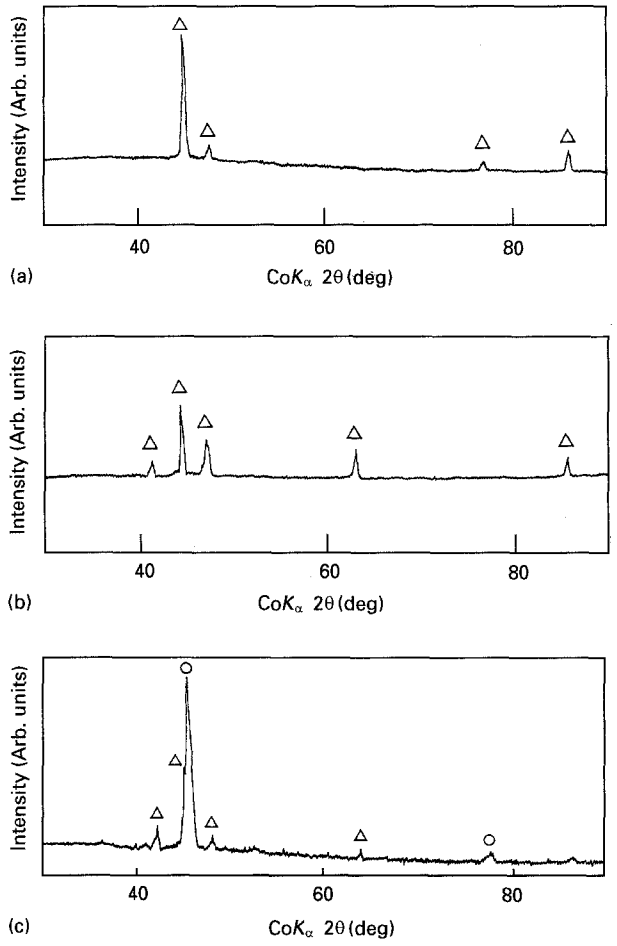

Figure 5 X-ray diffraction patterns obtained from the laser surface-melted zones: traverse speeds (a) 33.3 mm s^{-1}, (b) 16.7 mm s^{-1}, (c) 13.3 mm s^{-1}. (○) γ, (△) α_2.

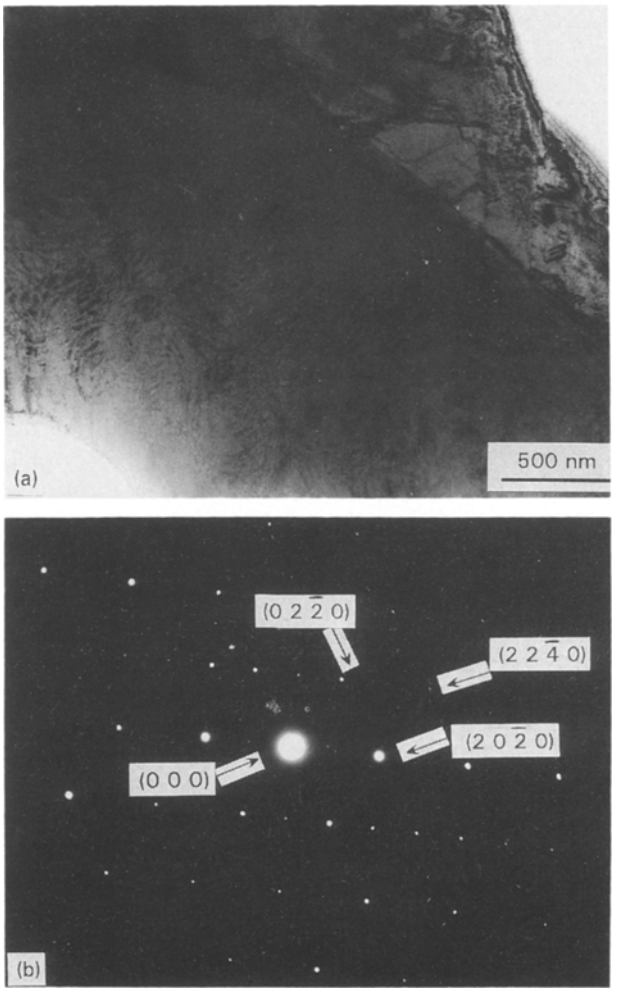

Figure 6 Transmission electron micrographs of the laser surface-melted zone (traverse speed 13.3 mm s^{-1}): (a) bright-field image of α_2 grain; (b) selected-area diffraction pattern of (a), (beam $\parallel [0001]_{\alpha_2}$); (c) bright-field image of γ grain; (d) selected-area diffraction pattern of (c), (beam $\parallel [3\bar{3}2]_{\gamma}$).

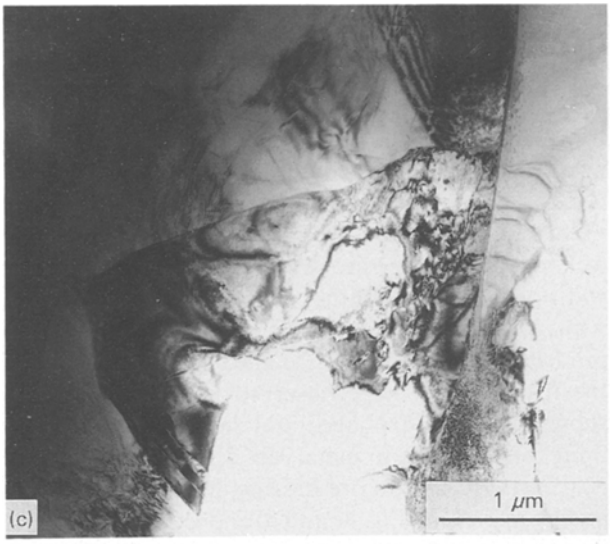

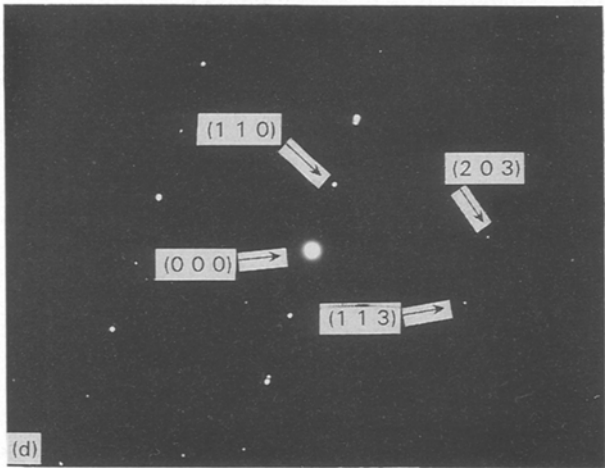

Figure 6 (continued)

ture, regardless of the traverse speed and the pre-heating temperature.

Fig. 10 shows average Vickers hardness values of the fusion zones produced by laser surface melting and laser welding are plotted against the traverse speeds. All the fusion zones were found to be harder than the base metal. In particular, the hardness of the fusion zones increased with the traverse speed, both in laser surface melting and laser welding. Thus, the hardness is considered to be related to the microstructures of the fusion zones.

3.2. Cracking

Many cracks were seen in all of the laser surface-melted zones. Most of the cracks were transverse cracks, which initiated in the fusion zone and propagated to the base metal. Similar weld cracking has been reported to occur in electron beam welds of Ti–48 mol % Al–6.5 vol % TiB_2 alloy [4]. The cracks are considered to be hot cracking which occurred in the solid state. In the laser welding, weld cracking was significantly reduced in comparison with laser surface melting. Table II shows the number of cracks observed in weld beads after the penetrant test. As clearly shown in this table, the crack reduced with decreasing traverse speed and increasing pre-heating temperature. As a result, laser welds without cracking could

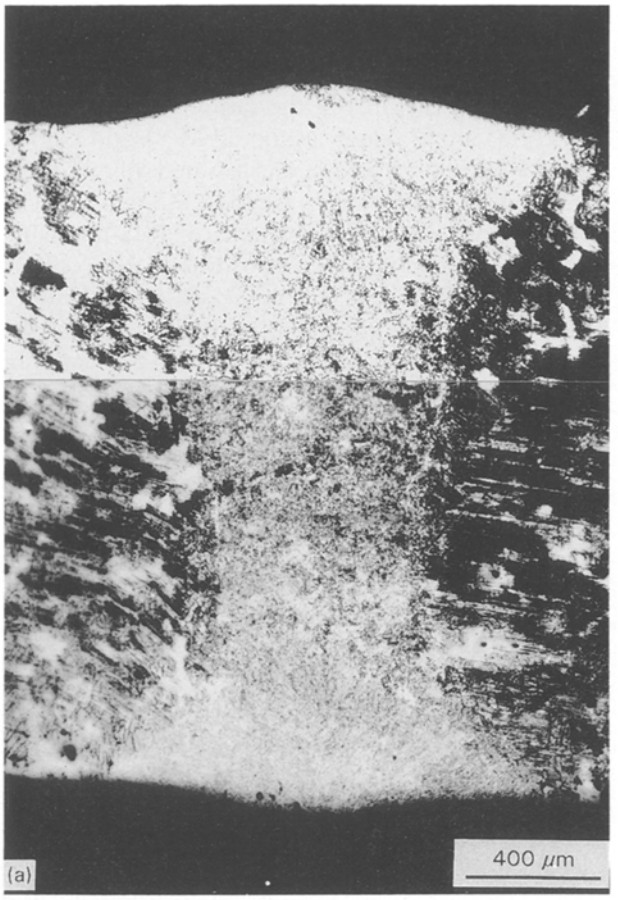

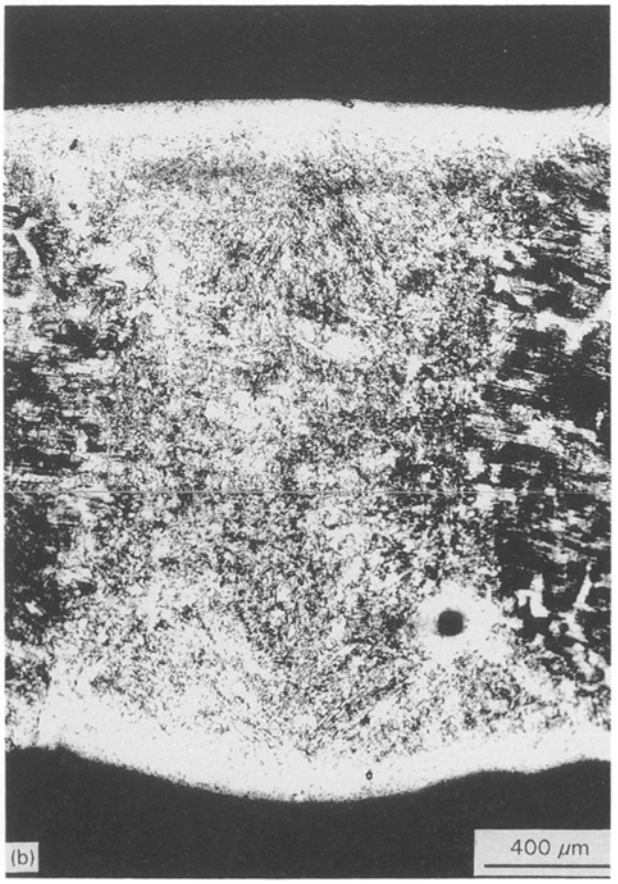

Figure 7 Cross-sectional optical micrographs of the laser-welded zones. Traverse speeds: (a) 50.0 mm s^{-1} without pre-heating; (b) 33.3 mm s^{-1} without pre-heating; (c) 50.0 mm s^{-1} with pre-heating of 673 K.

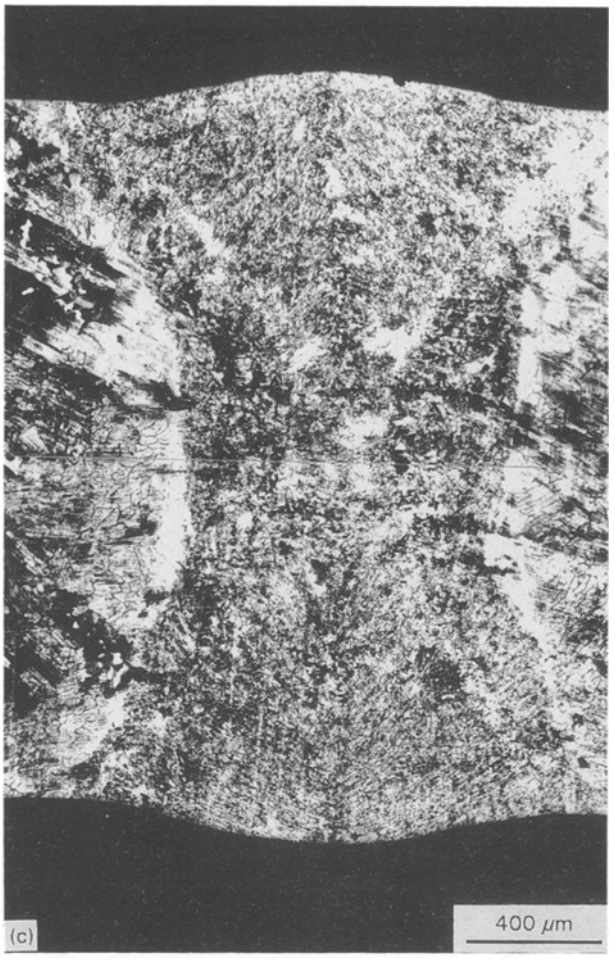

Figure 7 (continued)

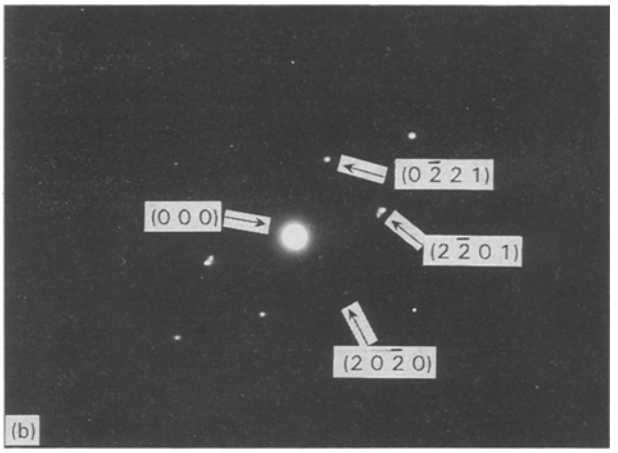

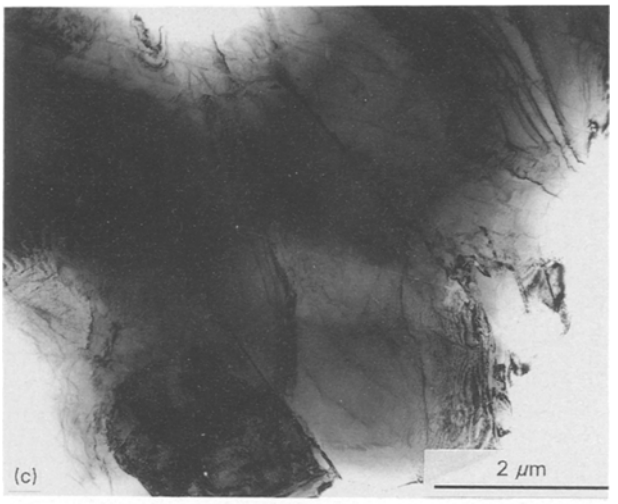

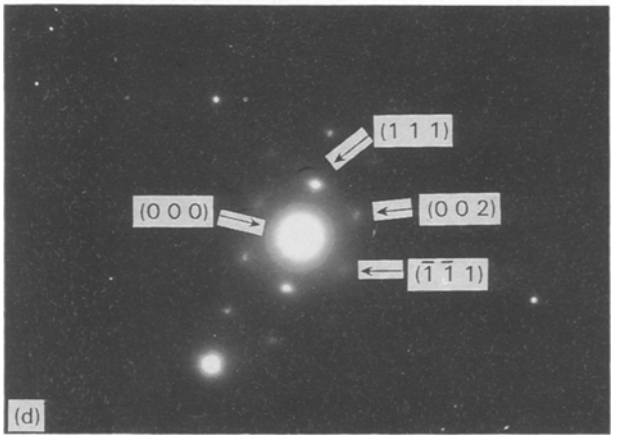

Figure 8 (continued).

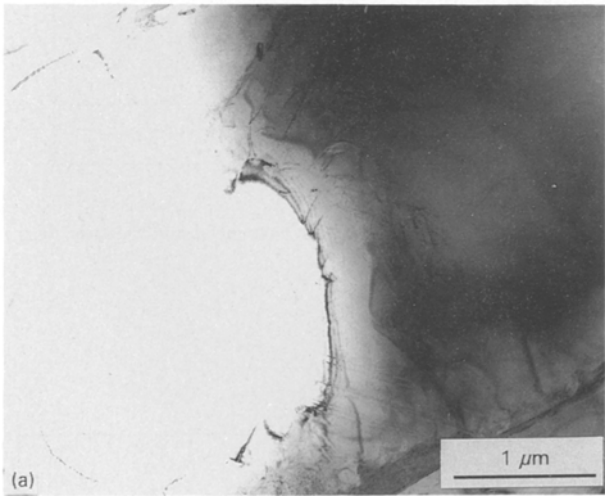

Figure 8 Transmission electron micrographs of the fusion zone of the laser weld (traverse speed 50.0 mm s^{-1} without pre-heating): (a) bright-field image of massive α_2; (b) selected-area diffraction pattern of (a), (beam ∥ $[0\,1\,1\,2]_{\alpha_2}$); (c) bright-field image of massive γ, (d) selected-area diffraction pattern of (c), (beam ∥ $[1\,\bar{1}\,0]_{\gamma}$); (e) bright-field image of lamellar structure.

be obtained at traverse speeds below 50.0 mm s^{-1} and pre-heating temperatures above 573 K.

3.3. Tensile test

Tensile tests were performed on the base metal and the laser weld without cracking. Two specimens were tested for each. Fig. 11 shows the result. Both of the specimens of the laser welds were fractured in the base metal. Thus, a weld joint with a joint efficiency of more than 100%, can be obtained by laser welding.

4. Discussion

4.1. Microstructure of the laser fusion zones

Microstructures and hardness of the laser fusion zones were significantly changed by the traverse speed and pre-heating temperature, as mentioned above. This should be related to cooling rates in the laser fusion zones, because solid-state transformations, $\alpha \rightarrow \alpha + \gamma$ and $\alpha \rightarrow \alpha_2$, being represented in the Ti–Al binary

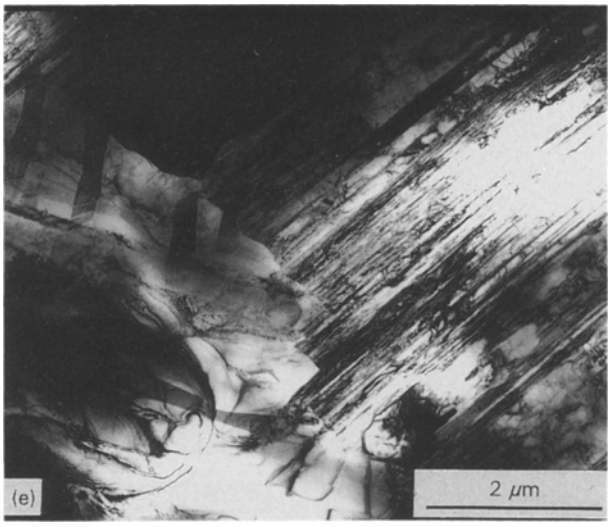

Figure 8 (continued)

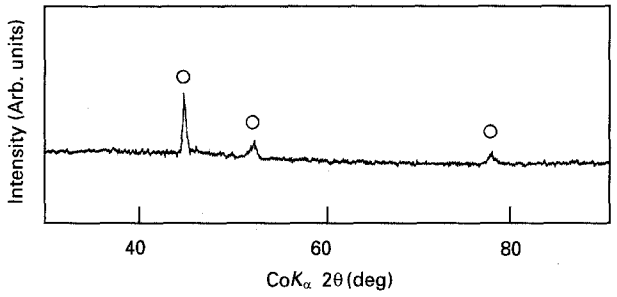

Figure 9 X-ray diffraction pattern obtained from the fusion zone of the laser weld (traverse speed 50.0 mm s^{-1} without pre-heating). (○) γ, (△) α_2.

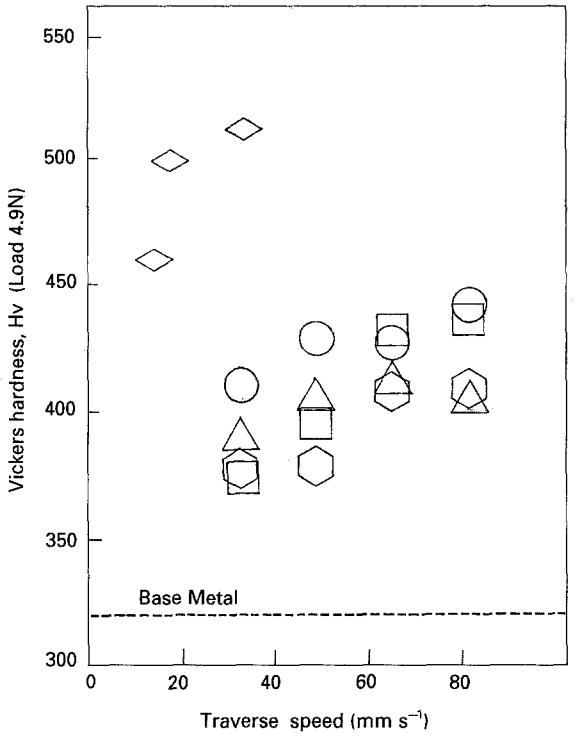

Figure 10 Average Vickers hardness values of the fusion zones produced by ◇ laser surface melting and laser welding: (○) no pre-heat, (□) 473 K preheat, (△) 573 K preheat, (⬡) 673 K preheat.

TABLE II Number of cracks observed in weld beads after the penetrant test

	Traverse speed (mm s^{-1})			
	33.3	50.0	66.7	83.3
No preheat	1	4	4	9
473 K preheat	1	1	3	5
573 K preheat	0	0	2	2
673 K preheat	0	0	1	1

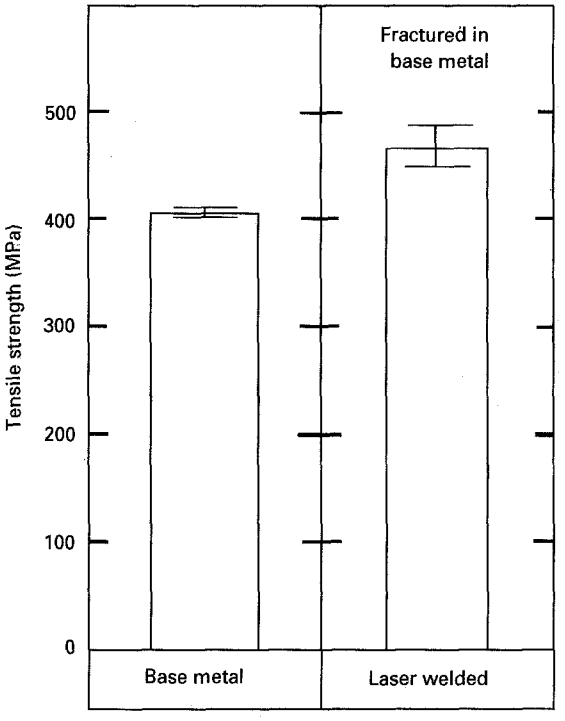

Figure 11 Tensile strengths of the base metal and the laser weld.

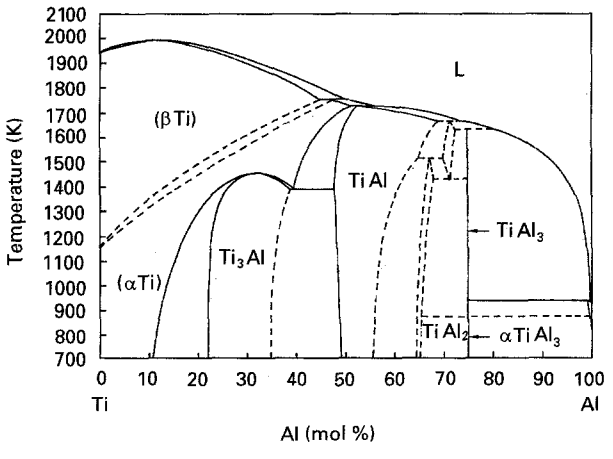

Figure 12 Ti–Al binary phase diagram.

system (Fig. 12) [5], should be affected by cooling rates. In this work, the cooling rates for laser surface melting and laser welding are calculated using the Rosenthal equations [6] for three-dimensional and two-dimensional heat flow, respectively.

For three-dimensional heat flow, the cooling time from T_1 to T_2, $CT_{T_1-T_2(3)}$, at a point on the centreline of the bead surface is given by

$$CT_{T_1-T_2(3)} = \frac{Q}{2\pi\lambda v}\left[\frac{1}{(T_2 - T_0)} - \frac{1}{(T_1 - T_0)}\right] \quad (1)$$

where v is the traverse speed ($m\,s^{-1}$), Q the heat input (W), λ the thermal conductivity ($W\,m^{-1}\,K^{-1}$) and T_0 the initial temperature of the plate (K). The heat input, Q, is estimated to be 30% of the incident laser power for laser surface melting. The thermal conductivity, λ, of TiAl is $20\,W\,m^{-1}\,K^{-1}$. The initial temperature of the plate is 283 K.

For two-dimensional heat flow, the cooling time from T_1 to T_2, $CT_{T_1-T_2(2)}$, at a point on the centreline of the bead surface, is given by

$$CT_{T_1-T_2(2)} = \frac{1}{4\pi\lambda c\rho}\left(\frac{Q}{hv}\right)^2\left[\frac{1}{(T_2 - T_0)^2} - \frac{1}{(T_1 - T_0)^2}\right] \quad (2)$$

where c is the specific heat ($J\,kg^{-1}\,K^{-1}$), ρ the density ($kg\,m^{-3}$), and h the plate thickness (m). The heat input, Q, is estimated to be 90% of the incident laser power for laser welding. The specific heat of TiAl is $0.5 \times 10^3\,J\,kg^{-1}\,K^{-1}$, its density is $3.84 \times 10^3 kg\,m^{-3}$ and the plate thickness is 2.0×10^{-3}m.

Because the cooling rates over the temperature range where the solid-state transformations occur should affect the microstructure of the fusion zone, average cooling rates between 1773 and 1273 K were calculated using Equations 1 and 2. The microstructures of the surface-melted zones and the welded zones with various laser parameters represented in the results, can be systematically classified using the cooling rates. Table III shows the relationship between the cooling rates and the microstructures of the fusion zones. The phases formed in the fusion zones were changed in the following way as the cooling rate increased:

massive α_2 + massive γ + lamellar $\rightarrow$

massive α_2 + massive $\gamma \rightarrow \alpha_2$.

TABLE III Relationship between the cooling rates and the microstructures of the fusion zones

Average cooling rate from 1773–1273 K ($K\,s^{-1}$)	Microstructure
8210[a]	α_2
4127[a]	α_2
3287[a]	$\alpha_2^c + \gamma^d$
834[b]	$\alpha_2^c + \gamma^d + L$
490[b]	$\alpha_2^c + \gamma^d + L$
244[b]	$\alpha_2^c + \gamma^d + L$

[a] Laser surface melting.
[b] Laser welding.
[c] α_2^c, massive α_2.
[d] γ^c, massive γ.
L lameller

At a much slower cooling rate, the fusion zone will, of course, show full lamellar structure, which was seen in the base metal.

The solidification and solid-state transformations of alloys containing near 46 mol % Al are as follows, according to the phase diagram (Fig. 12):

$$L \rightarrow L + \beta \rightarrow L + \alpha \rightarrow \alpha \rightarrow \alpha + \gamma \rightarrow \alpha_2 + \gamma.$$

It has been reported that the transformation of $\alpha \rightarrow \gamma$ was suppressed by a rapid cooling for a Ti–46 mol % Al alloy [7]. However, the ordering of $\alpha \rightarrow \alpha_2$ occurred upon rapid cooling [7]. In this work, the single-phase structure of α_2 was seen in the fusion zones with cooling rates above $4000\,K\,s^{-1}$. In this case, therefore, it is considered that the $\alpha \rightarrow \gamma$ transformation was suppressed and subsequently α was ordered.

The microstructures of the fusion zones with cooling rates below $4000\,K\,s^{-1}$ consisted of α_2 and γ in massive form. Kumagai *et al.* [8] have reported that an almost single-phase structure of γ was obtained by quenching in ice–water from the α region for a Ti–48 mol % Al alloy. This has been reported to be caused by a massive transformation of α to γ which occurred in the $\alpha + \gamma$ region. In the present case, therefore, massive γ is considered to be formed by the massive transformation of α to γ prior to the ordering of α. Subsequently, residual α phase may be ordered. Thus the $\alpha_2 + \gamma$ structure seems to be formed in the fusion zones. On the basis of the above-mentioned considerations, the continuous cooling phase diagram for the alloy used in this work is schematically represented in Fig. 13.

The relationship between the cooling rates and average Vickers hardness values of the fusion zones is shown in Fig. 14. The hardness obviously increased with increasing cooling rate. This is thought to be because α_2, which is harder than γ, became dominant as the cooling rate increased. The single-phase structure of α_2 showed a hardness above 500 Hv. As a result, it is concluded that the fusion zones and heat-affected zones heated into the α region in the TiAl alloy, harden upon rapid cooling.

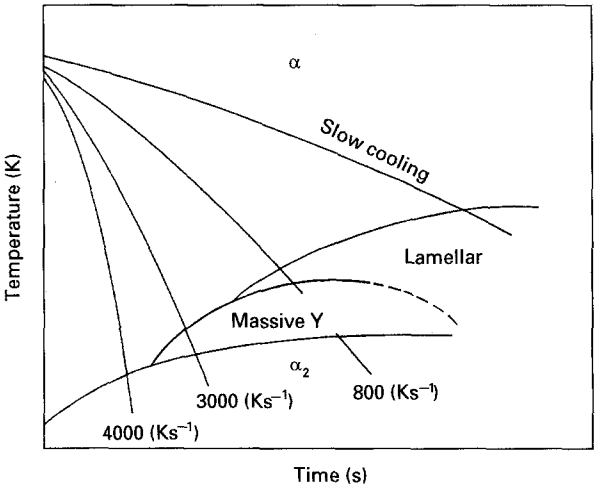

Figure 13 Schematic CCT diagram for Ti–46 mol % Al–2 mol % Mo alloy.

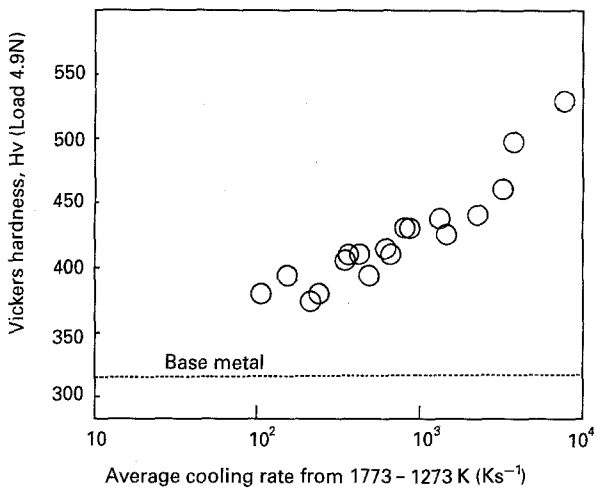

Figure 14 Relationship between the average cooling rates from 1773–1273 K and Vickers hardness of the laser fusion zones.

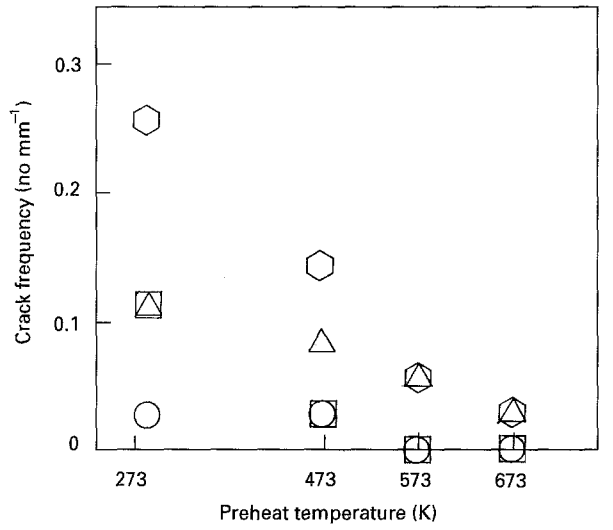

Figure 15 Crack-frequency values plotted as functions of pre-heating temperature and traverse speed: (○) 33.3 mm s^{-1}, (□) 50.0 mm s^{-1}, (△) 66.7 mm s^{-1}, (⬡) 83.3 mm s^{-1}.

4.2. Weldability of Ti–46 mol % Al–2 mol % Mo

The crack sensitivity of Ti–46 mol % Al–2 mol % Mo laser welds was characterized by crack frequency, defined as the number of cracks per unit millimetre of weld bead. Fig. 15 shows crack frequency values plotted as functions of pre-heating temperature and traverse speed. It is obvious from this figure that crack frequency decreased with increasing pre-heating temperature and decreasing traverse speed. In other words, the crack sensitivity of laser welds decreased as the cooling rates decreased.

Cracking occurs when thermal strains exceed the ductility of weld beads upon cooling. Consequently, the cooling rates are considered to have two possible effects on the crack sensitivity. First, high cooling rates result in hardening of the fusion zones, which reduces their ductility. This can enhance the crack sensitivity. Fig. 16 shows the relation between the crack-sensitivity values and average hardness values of the weld beads. Cracking significantly decreased when the

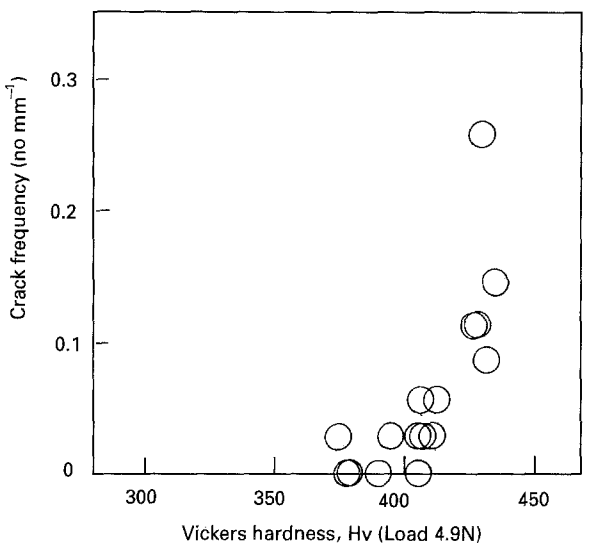

Figure 16 Crack-frequency values versus Vickers hardness of the laser fusion zones.

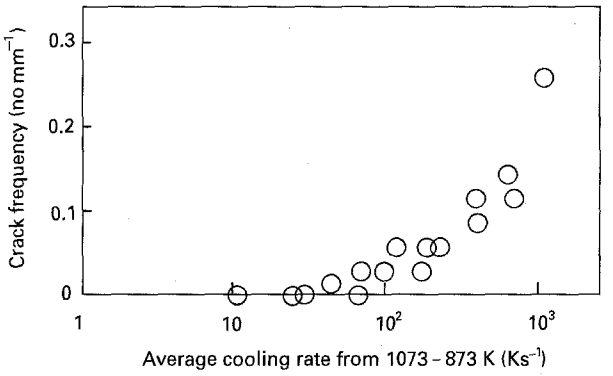

Figure 17 Crack-frequency values versus average cooling rates from 1073–873 K.

hardness was reduced below 400 Hv. Second, increasing cooling rates induce higher thermal strain rates in a temperature range of reducing ductility, which may lead to higher crack sensitivity. Ductility of TiAl has been reported to be reduced severely in temperatures below 973 K [9]. Thus, cooling rates across 973 K are thought to be related to cracking. So the average cooling rates between 1073 and 873 K are calculated from Equation 2 and crack-frequency values are plotted against the cooling rates in Fig. 17. No cracking occurred in a cooling rate below approximately 30 K s^{-1}. Therefore, the critical cooling rate to prevent cracking is found to be 30 K s^{-1}.

Because these two effects of the cooling rates do not independently affect the crack sensitivity, it cannot be decided which is the dominant factor. As a result, successful laser welding of Ti–46 mol % Al–2 mol % Mo without cracking can be obtained when optimum welding parameters, which result in an average cooling rate between 1073 and 873 K below approximately 30 K s^{-1} and hardness of the fusion zones below approximately 400 Hv, are selected. Moreover, the weld joints without cracking have a joint efficiency of more than 100%. Therefore, laser welding can be applied to the joining of the TiAl alloy.

5. Conclusions

Laser surface melting and laser welding were performed on Ti–46 mol % Al–2 mol % Mo using a 2.5 kW CO_2 laser. The results obtained are as follows.

1. In laser surface melting, single-phase structure of α_2 was seen in the fusion zones when the calculated cooling rates between 1773 and 1273 K were above 4000 $K\,s^{-1}$. In this case, it is considered that the $\alpha \rightarrow \gamma$ transformation was suppressed and subsequently α was ordered. The microstructures of the fusion zones with the cooling rates below 4000 $K\,s^{-1}$ consisted of α_2 and γ in massive form. Massive γ may be formed by the transformation of α to γ prior to the ordering of α. Subsequently, residual α may be ordered. In laser welding, the microstructure of the fusion zones was mainly composed of massive α_2 + massive γ + lamellar.

2. The average hardness of the fusion zones increased with increasing cooling rates and the single-phase structure of α_2 showed hardness above 500 Hv. This is because α_2, which is harder than γ, became dominant as the cooling rate increased.

3. All of the laser surface-melted zones included cracking. In laser welding, cracking was reduced with decreasing traverse speed and increasing pre-heating temperature. Crack-free welds could be obtained at traverse speeds below 50.0 $mm\,s^{-1}$ and pre-heating temperatures above 573 K.

4. Crack sensitivity was related to the cooling rates over the temperature range of reducing ductility and the microstructure of the fusion zones. As a result, cracking was prevented by selecting the optimum welding parameters which result in a calculated cooling rate between 1073 and 873 K below approximately 30 $K\,s^{-1}$ and the hardness of the fusion zones below approximately 400 Hv.

5. In tensile tests, the laser-weld specimens without weld cracking were fractured in the base metal. Thus a weld joint having a joint efficiency of more than 100% can be obtained using laser welding.

References

1. K. HASHIMOTO, H. DOI, K. KASAHARA, T. TSUJIMOTO and T. SUZUKI, *J. Jpn Inst. Metals* **52** (1988) 816.
2. K. NONAKA, K. TONOZAKI, M. FUJITA, A. CHIBA, T. KAWABATA and O. IZUMI, in "Abstract Bulletin, 104th Meeting of the Japanese Institute of Metals", Yokohama, Japan, (JIM, 1989) p. 329.
3. T. MAEDA, M. OKADA and Y. SHIDA, "High-Temperature Ordered Intermetallics IV", Materials Research Symposia Proceedings edited by L. Johnson, J. O. Stiegler and D. P. Pope (1991) 777.
4. R. A. PATTERSON, P. L. MARTIN, B. K. DAMKROGER and L. CHRISTODOULOU, *Weld. J.* **69** (1990) 39-S.
5. M. McCULLOUGH, J. J VALENCIA, C. G. LEVI and R. MEHRABIAN, *Acta Metall.* **37** (1989) 1321.
6. D. ROSENTHAL, *Weld. J.* **20** (1941) 220-S.
7. E. L. HALL and SHYH-CHIN HUANG, *Acta Metall.* **38** (1990) 539.
8. T. KUMAGAI, M. TAKEYAMA and M. NAKAMURA, "Abstract Bulletin, 111th Meeting of the Japanese Institute of Metals", Toyama, Japan (JIM, 1992) p. 272.
9. Y. NISHIYAMA and S. ISOBE, "High Temperature Aluminides and Intermetallics" (TMS, Warrendale, PA, 1990) p. 557.

Received 13 October 1993
and accepted 27 July 1994